EUROPEAN ORGANISATION FOR NUCLEAR RESEARCH

EPS0507
Pa: 10
Pl: 1

FIRST MEASUREMENT OF THE QUARK-TO-PHOTON FRAGMENTATION FUNCTION

The ALEPH Collaboration

Abstract

Earlier measurements at LEP of isolated hard photons in hadronic Z decays, attributed to radiation from primary quark pairs, have been extended in the ALEPH experiment to include hard photon production *inside* hadron jets. Events are selected where all particles combine democratically to form hadron jets, one of which contains a photon with a fractional energy $z \geq 0.7$. After statistical subtraction of non-prompt photons, the quark-to-photon fragmentation function, $D(z)$, is extracted directly from the measured 2-jet rate. By taking into account the perturbative contributions to $D(z)$ obtained from an $\mathcal{O}(\alpha\alpha_S)$ QCD calculation, the unknown non-perturbative component of $D(z)$ is then determined at high z. Provided due account is taken of hadronization effects near $z = 1$, a good description of the other event topologies is then found.

Contribution to the International Europhysics Conference on High Energy Physics
Brussels, Belgium, July 27 - August 2, 1995

1 Introduction

Several studies have been made of the production of hard isolated prompt photons accompanying hadronic decays of the Z at LEP [1]. The origin of these photons has been attributed to final state radiation (FSR) emitted at an early stage in the QCD parton evolution process initiated from the primary quark-antiquark pair. The main thrust of this work has been to compare the data with QCD $\mathcal{O}(\alpha\alpha_S)$ calculations at the parton level [2, 3] and to test the detailed predictions of the parton shower models, `JETSET` [4], `HERWIG` [5] and `ARIADNE` [6] and thus gain some insight into the parton evolution mechanism.

In all these analyses, the candidate photon was isolated from the hadronic debris in an event using a geometrical cone centred around its direction inside of which a minimal residue of accompanying hadronic energy was allowed. This procedure was considered necessary to reduce the non-prompt photon backgrounds from hadron decays. In the next step, the photon was removed from the event before jets were formed with the other particles using a clustering recombination algorithm. The consequence was that any particles associated with the photon were incorporated into the other jets. Finally, an event was retained only if the restored candidate photon remained apart from the jets in a second application of the clustering algorithm. Early measurements using this "two-step" approach revealed large apparent discrepancies with the available QCD predictions in the particular case of events with a γ + 1-jet topology. It was soon realised that this was due to an inadequate definition of phase space boundaries where they are close to collinear singularities in the theoretical parton level cross sections [7]. Even when these difficulties were understood, the various QCD calculations [2, 3] required large α_s dependent corrections to approach the data.

It was pointed out [2] that a safer approach would be to apply a jet recombination scheme simultaneously to all particles in an event, including the photon. This "democratic" approach enables the phase space regions for all event topologies to be properly defined and handles correctly those hadrons which are associated naturally with the photon. However, it introduces a significant non-perturbative contribution to the cross section which depends upon the amount of accompanying energy allowed in the "photon jet". At first sight, this would appear to prevent the accurate comparison of data with the QCD predictions employed earlier. The purpose of this paper is to show that a significant part of the parton-to-photon fragmentation function can be measured, allowing this non-perturbative contribution to be determined. This adds new information to the dynamics of quark radiation, and at the same time improves the comparison of all FSR data with the QCD calculations.

In this study, a sample of 1.17 million selected hadronic Z decay events are subdivided into 2-jet, 3-jet and $\geq$ 4-jet topologies using the DURHAM E0 algorithm [8] with the resolution parameter, y_{cut}, varied between 0.001 and 0.33. Events are kept where at least one of the reconstructed hadron jets contains a photon ($E_\gamma > 5$ GeV) carrying at least 70% of the total energy of the jet. The fractional energy, z_γ, of such a photon within a

jet is defined as:

$$z_\gamma = \frac{E_\gamma}{(E_\gamma + E_{had})}$$

where E_{had} is the energy of all accompanying hadrons in the "photon-jet" found by the clustering algorithm. Thus, events with completely isolated photons appear at $z_\gamma = 1$. Currently, the measured z_γ range is limited to $0.7 < z_\gamma < 1.0$ by residual hadronic decay backgrounds which are large for the 2-jet sample, i.e. events with a single hadron-jet + photon-jet topology. These backgrounds are subtracted statistically according to Monte Carlo predictions after direct experimental confirmation that the principal components, namely the inclusive π^0 rates, are adequately simulated.

In this paper, the measured differential z_γ distribution thus obtained from the 2-jet event sample is used to determine directly the quark-to-photon fragmentation function, $D(z_\gamma)$, above $z_\gamma = 0.7$. This permits a direct comparison with theoretical predictions by Duke and Owens [9] used to determine quark bremsstrahlung background to prompt photon production at the hadron colliders. Recently, it has been shown in an $\mathcal{O}(\alpha\alpha_S)$ QCD calculation by Glover and Morgan [10] that the perturbative contributions to $D(z_\gamma)$ can be evaluated, thus allowing the non-perturbative part of the $D(z_\gamma)$ function to be determined from the data.

The above $\mathcal{O}(\alpha\alpha_S)$ QCD calculation postulates that the non-perturbative part of the $D(z_\gamma)$ function is described by an evolution equation with appropriate coefficients such that, when added to the perturbative contributions at the same order, any dependence on the arbitrarily chosen factorisation scale is eliminated. However, this equation requires a starting value at some given mass scale, μ_0, to be fully specified. Below this cut-off mass scale, the evolution equation no longer describes the behaviour of the cross section. Direct fitting of the predictions of this formalism to the measured $D(z_\gamma)$ function shows that a simple solution for the evolution equation with μ_0 as the only free parameter can be found.

The same QCD $\mathcal{O}(\alpha\alpha_S)$ calculation predicts the perturbative isolated photon component at $z_\gamma = 1$ for 2, 3 and $\geq$4-jet event topologies. With a suitable choice of α_S for the 3 and $\geq$4-jet event rates, these predictions are in good agreement with the data over a wide range of y_{cut}.

2 Selection of Events with Final State Photons

2.1 Hadronic event selection

The components of the ALEPH detector used in this analysis are described in Ref [11]. The hadronic Z decays are selected using standard procedures described in detail elsewhere [12] where at least 5 charged tracks are measured in the Time Projection Chamber (TPC), their summed energy being greater than $10\%\sqrt{s}$. This selects a total sample from 1990-1992 data of 1 170 849 events recorded at centre of mass energies between 88.25 and 94.25 GeV, 88% of which are at 91.2 GeV.

The thrust axis of each event is computed using all the "energy flow objects" [13] found. These objects are derived from all reconstructed charged particles, photons and

neutral hadronic energy depositions in the electromagnetic (ECAL) and hadronic (HCAL) calorimeters, where due account is taken of redundancy in their corresponding momentum and energy measurements. At the Z, a Gaussian fit to the total reconstructed energy gives a peak value of 90.5 GeV with a resolution of 6.2 GeV, which is well reproduced by Monte Carlo simulation. The event is kept if $|\cos\theta_{thrust}| < 0.95$ where θ_{thrust} is the polar angle of the thrust axis with respect to the beam axis.

2.2 Selection of single photon clusters

The photon selection begins with the identification of neutral electromagnetic clusters in the ECAL with energies greater than 5 GeV. Clusters reconstructed close to cracks between calorimeter modules, within the overlap region between barrel and endcaps, and at polar angles for which $|\cos\theta_\gamma| > 0.95$ are rejected. An algorithm is then employed [13] which uses the fine granularity and longitudinal segmentation of the ECAL to recognise compact neutral objects within the clusters. Since the main background of the analysis arises from energetic π^0s where the decay photons overlap to form a single cluster, a large fraction are removed by requiring that only one compact object can be recognised in any candidate cluster. Further rejection of π^0s is achieved by a moments analysis of the energy sharing between neighbouring detector elements within the single object cluster. A normalised estimator, σ_L, which has a Gaussian shaped distribution, centred at zero with unit width, is formed from the measured major axis of the moments ellipse. From a study of real and simulated $e^+e^- \to \ell^+\ell^-\gamma$ events, this estimator is found to be independent of the energy and polar angle of the photon. Only clusters which satisfy $-3 < \sigma_L < 2$ are kept. This selection removes about 3/4 of the π^0 background at 32 GeV reducing to about 1/3 at 43 GeV.

The efficiency of this single photon selection has been determined using a sample of 23 000 fully simulated events from `ARIADNE3.3` each containing a FSR photon with an energy greater than 5 GeV. The overall efficiency is $55.0 \pm 2.4\%$ almost independent of the energy of the photon and takes into account the effect of neighbouring particles. The losses are: 8% coming from photon conversions, 5% from the $|\cos\theta_\gamma|$ cut, 15% due to cracks and the overlap region, and 7% where the photon is merged with other objects. The remaining loss of 10% is due to the single photon selection cuts.

2.3 Selection of final state radiation events

For each event with at least one selected photon, jets are then constructed using all the energy flow objects of the event and treating the photon equally with all the other particles. The particle clustering is performed using the DURHAM E0 algorithm. For each pair of particles i and j in an event, the quantity y_{ij} is defined:

$$y_{ij} = (M_{ij}/E_{vis})^2 \quad \text{with} \quad M_{ij}^2 = 2\min(E_i^2, E_j^2)(1-\cos\theta_{ij})$$

where E_i and E_j are their energies, θ_{ij} their opening angle, and E_{vis} the total visible energy in the event. The particles are combined as long as y_{ij} is smaller than the specified jet resolution parameter y_{cut}. The number of jets is then the number of surviving particle

clusters. The event is kept if at least one jet contains a selected photon with $z_\gamma > 0.7$. This procedure is repeated successively for 13 different y_{cut} values increasing from 0.001 to 0.33.

For each value of y_{cut}, the event sample is then divided into three categories corresponding to jet topologies of 2, 3 and ≥ 4 jets (ie an event with more than 4 jets is classified as 4-jets), where the number of jets includes the photon jet. Fig. 1 shows the observed z_γ distributions at $y_{cut} = 0.01$ subdivided by jet topology and compared with the predictions of `JETSET7.3`; the large background for 2-jet events is quite evident. In the following analysis, the z_γ distribution is divided into 6 equal bins between 0.7 and 1 for each topology. In order to separate more clearly the large contribution coming from the isolated photon component near $z_\gamma = 1$, the last bin is split into two parts: $0.95 < z_\gamma < 0.99$ and $0.99 < z_\gamma \leq 1$. The experimental uncertainty in z_γ for 2-jet events near $z_\gamma = 1$ is determined by the objects with energies below threshold for detection. These thresholds are 250 MeV for neutral objects and somewhat less for charged particles, implying a maximum uncertainty in z_γ of 0.005 per missing object. For 3-jet and 4-jet events, the mean jet energy is lower, so that the threshold effects are more pronounced and account for the dips observed near $z_\gamma = 1$ in the corresponding z_γ distributions.

3 Background Subtraction and Systematic Errors

Simulation of hadronic decays from the Z in the detector shows that the principal source of background is still multi-photon clusters which remain indistinguishable from single photons, and to a lesser extent initial state radiation (ISR) from the incoming leptons. The former arises mainly from the electromagnetic decays of hadrons and is a strong function of the topology of the event and z_γ as highlighted in Fig. 1, whereas ISR concentrates at high z_γ. These backgrounds are determined by Monte Carlo simulations and subtracted statistically from the data bin-by-bin in z_γ for each value of y_{cut}. The assessment of the dominant systematic errors in these procedures is described below.

3.1 Non-prompt Photons from Hadron Decays

The contribution from non-prompt photons, mainly π^0s, is determined from a sample of 1.95 million fully simulated events generated using `JETSET7.3` with fragmentation parameters tuned to the properties of hadronic events measured in ALEPH [14]. Two independent experimental methods are applied to determine the precision of the Monte Carlo simulation for π^0 production, both employing the same selected data sample of 1.17 million hadronic events.

In the first method, V^0s identified as low mass e^+e^- pairs are combined with single neutral electromagnetic clusters with energies above 5 GeV to search for π^0s. The simulation of such V^0s, which arise from photon conversions in the materials around the interaction point, follows closely the rate and source distribution observed. Thus, the ratio of selected $e^+e^-\gamma$ combinations observed to those predicted is a measure of the accuracy of π^0 production in `JETSET`. After selecting only those combinations with energies above 30 GeV, corresponding to $z_\pi > 0.7$ for 2- jet events, clearly resolved π^0 (and η) peaks are

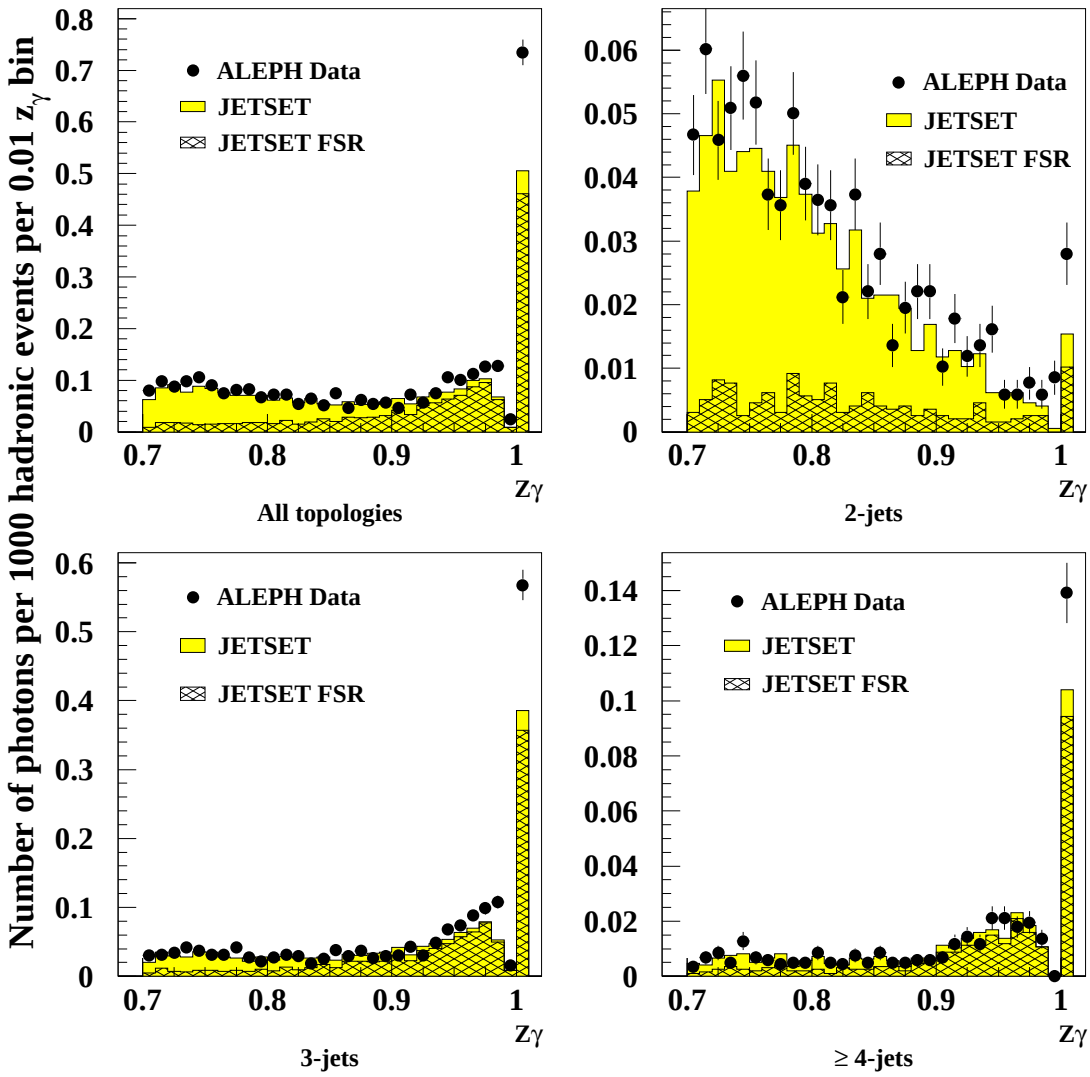

Figure 1: Observed z_γ distributions at $y_{cut} = 0.01$ in each topology before background subtraction. The cross-hatched areas show the signal component in the JETSET Monte Carlo selected samples.

formed in the data and Monte Carlo from which the ratio of π^0s observed is found to be 1.04 ± 0.12. Fig. 2 (upper) shows that their relative distributions in the defined z_π bins are also consistent, although errors are large due to low statistics.

The second method gives better precision in the highest z_π bins. All the parton shower programs predict that the π^0 fragmentation function is equal to the average of the charged pions for $z_\pi > 0.7$. Their production is dominated by primary light quark fragmentation and the decays of the ρ resonance which are isospin symmetric. Inclusive charged pion production has been studied in ALEPH [15] from hadronic Z decays, where all charged hadrons are separated statistically into pions, kaons and protons using dE/dx measurements in the TPC. This analysis has been extended to cover all z_π bins up to the kinematic limit, with enhanced statistics. The minimum number of hits required per track in all detectors is increased so that momenta are determined to better than 3% and the fraction of badly measured tracks (from "kinks" and misassociated hits) substantially reduced. On average 53% of accepted tracks with $z_\pi > 0.7$ are identified as pions after fitting the dE/dx spectra observed in each z_π bin. The small contamination of electrons and muons in the pion sample ($\leq 1.4\%$) is subtracted using the Monte Carlo. The measured differential z_π rate of identified $\pi^\pm$s is compared with the predictions of the Monte Carlo sample. Their ratio is compatible with being constant in z_π as shown in Fig. 2 (lower) with a mean value of 1.02 ± 0.03. The quoted errors include the systematic uncertainties in the simulation of the track selections, reconstruction efficiencies and dE/dx measurements.

Thus, the conclusion is that the Monte Carlo sample employed to subtract non-prompt backgrounds gives an adequate description of π^0 production, but a systematic uncertainty remains to be determined in the fraction of those π^0s which are rejected by the sequence of selection cuts described earlier. These errors are determined by comparing data and Monte Carlo rejection factors as a function of cluster energy and their respective evolution with cut location (σ_L). The rejection factors agree within statistics allowing a relative uncertainty of 6.5% to be assigned overall which is then added in quadrature to the uncertainties in π^0 production determined above.

The background from $\eta \to \gamma\gamma$ is included as given by the Monte Carlo. Its production is smaller than the π^0 and the single photon selection rejects it efficiently. The predicted contribution from JETSET is of the order of at most 2%, and is found to be in qualitative agreement with the data as observed from the yields of the reconstructed $e^+e^-\gamma$ events described earlier.

A much smaller background from neutral hadrons (ie neutrons,K^0s) misidentified as photons in ECAL is also determined by the same Monte Carlo. This background is about 2% for 2-jet topologies below $z_\gamma = 0.9$ independent of y_{cut} and is very small for all the others.

3.2 Initial State Radiation

Since ISR photons are mainly isolated, this background is very small for $z_\gamma < 0.90$ but becomes the dominant background for $z_\gamma > 0.99$. Its contribution to the total data sample is approximately independent of y_{cut} and event topology, being at the level of 5–10% for $z_\gamma > 0.99$, and about 1% for $z_\gamma < 0.90$. The relative systematic error in the ISR rate is

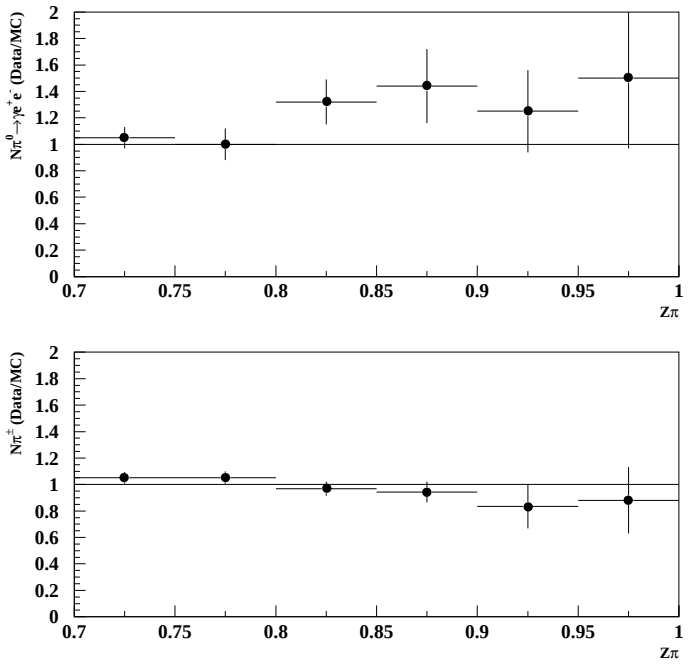

Figure 2: Ratios of number of pions found in the data and the Monte Carlo by the π^0 selection with a converted photon (upper) and by the $\pi^\pm$ selection (lower).

assigned to be 5% [1].

3.3 $Z \to \tau^+\tau^-$

This background is estimated by applying the selection on 130 000 fully simulated $Z \to \tau^+\tau^-$ events, generated using KORALZ [16]. It arises from high multiplicity τ decays with an ISR photon or photons from π^0 decay and contributes typically 2–3% to the selected inclusive photon sample in the 2-jets topology, $\leq 1\%$ in the 3-jets topology for $0.7 < z_\gamma < 0.99$ and 2% for $z_\gamma > 0.99$. It is completely negligible in the $\geq$ 4-jet topology.

3.4 FSR Signal Purity

The residue of the measured rate not accounted for after the statistical subtraction of all backgrounds described above is ascribed to FSR photons. Its relative rate defines the observed signal purity and is calculated for each event topology, y_{cut} and z_γ bin. Table 1 shows the integrated purities obtained for $z_\gamma > 0.7$ and $z_\gamma > 0.95$ respectively. As expected, the purity is low in the 2-jet case and strongly z_γ dependent.

y_{cut}	All events photon candidates	2-jet events photon cand.	2-jet events FSR purities	3-jet events photon cand.	3-jet events FSR purities	$\geq$ 4-jet events photon cand.	$\geq$ 4-jet events FSR purities
0.001	8756	326	$15.8 \pm 6.1\%$	1787	$51.2 \pm 1.7\%$	6643	$57.9 \pm 0.8\%$
0.002	6424	563	$15.5 \pm 4.7\%$	2428	$62.8 \pm 1.2\%$	3433	$67.3 \pm 0.9\%$
0.004	4950	793	$22.1 \pm 3.7\%$	2527	$67.7 \pm 1.1\%$	1630	$73.2 \pm 1.2\%$
0.006	4305	891	$22.1 \pm 3.5\%$	2405	$71.0 \pm 1.0\%$	1009	$76.3 \pm 1.4\%$
0.008	3902	971	$24.0 \pm 3.3\%$	2240	$72.8 \pm 1.0\%$	691	$77.5 \pm 1.7\%$
0.01	3604	1018	$23.8 \pm 3.2\%$	2110	$75.0 \pm 1.0\%$	476	$76.7 \pm 2.0\%$
0.02	2806	1158	$25.6 \pm 3.0\%$	1514	$78.0 \pm 1.1\%$	134	$77.9 \pm 3.7\%$
0.04	2269	1278	$27.3 \pm 2.8\%$	965	$81.2 \pm 1.2\%$	26	$85.8 \pm 6.7\%$
0.06	1988	1321	$27.9 \pm 2.7\%$	661	$81.4 \pm 1.5\%$	6	$79.4 \pm 19.\%$
0.08	1811	1354	$28.6 \pm 2.6\%$	455	$80.6 \pm 1.8\%$	2	$100.^{+0.}_{-88.}\%$
0.1	1710	1375	$28.9 \pm 2.6\%$	335	$82.2 \pm 2.0\%$	0	
0.2	1511	1448	$31.1 \pm 2.5\%$	63	$83.6 \pm 4.5\%$	0	
0.333	1466	1466	$32.0 \pm 2.5\%$	0		0	

y_{cut}	All events photon candidates	2-jet events photon cand.	2-jet events FSR purities	3-jet events photon cand.	3-jet events FSR purities	$\geq$ 4-jet events photon cand.	$\geq$ 4-jet events FSR purities
0.001	2613	16	$35.5 \pm 22.5\%$	550	$85.1 \pm 1.4\%$	2047	$87.8 \pm 0.7\%$
0.002	2266	32	$60.0 \pm 11.2\%$	908	$88.5 \pm 0.9\%$	1326	$89.9 \pm 0.7\%$
0.004	1945	48	$62.1 \pm 8.8\%$	1150	$90.6 \pm 0.7\%$	747	$89.6 \pm 1.0\%$
0.006	1730	55	$63.6 \pm 8.0\%$	1192	$91.8 \pm 0.7\%$	483	$90.8 \pm 1.2\%$
0.008	1569	67	$70.1 \pm 6.4\%$	1153	$92.7 \pm 0.6\%$	349	$92.6 \pm 1.2\%$
0.01	1445	73	$69.2 \pm 6.2\%$	1121	$93.6 \pm 0.6\%$	251	$92.1 \pm 1.5\%$
0.02	1082	95	$74.4 \pm 4.8\%$	910	$95.1 \pm 0.6\%$	77	$93.6 \pm 2.5\%$
0.04	768	123	$77.7 \pm 3.9\%$	627	$96.3 \pm 0.6\%$	18	$93.1 \pm 5.9\%$
0.06	589	137	$80.0 \pm 3.4\%$	448	$96.6 \pm 0.7\%$	4	$84.6^{+15.4}_{-22.}\%$
0.08	467	151	$81.8 \pm 3.1\%$	315	$96.0 \pm 0.9\%$	1	$100.^{+0.}_{-88.}\%$
0.1	396	164	$82.9 \pm 2.9\%$	232	$96.4 \pm 1.0\%$	0	
0.2	250	207	$85.6 \pm 2.3\%$	43	$96.1 \pm 2.4\%$	0	
0.333	221	221	$86.5 \pm 2.1\%$	0		0	

Table 1: Number of photon candidates selected in the data sample with (upper) $z_\gamma > 0.7$ and with (lower) $z_\gamma > 0.95$ respectively, and estimated FSR purities in each n-jet class; quoted errors are statistical only.

4 Acceptance Corrections to Hadron Level

In order to compare the data with the QCD matrix element predictions, after subtraction of all backgrounds, the measured n-jet rates in each z_γ bin are corrected for geometric acceptance, photon conversion losses and reconstruction inefficiencies. These corrections are determined using a sample of fully reconstructed hadronic events, each containing a FSR photon, generated with a parton shower Monte Carlo and processed with a detailed simulation of the ALEPH detector where the same 5 GeV cut on the reconstructed photon energy is applied. A sample of `ARIADNE` events corresponding to 2.7 million hadronic events is used for this. The acceptance corrections also include the effect of mixing of event topologies arising from the limitations of the detector.

For each reconstructed event at detector level where a FSR photon is measured in a given z_γ bin, an element (ij) of a 3×3 matrix, defined for this bin, is incremented if i and j jets are found at generator and detector levels respectively. At this stage, no constraint is placed on the z_γ value of the FSR photon at the generator level. After processing the full sample, the numbers of events found in each (ij) element are normalised by the total number of generated FSR photons found with i jets in the corresponding z_γ bin producing an acceptance matrix $\mathcal{P}_{i \to j}$ for each z_γ bin. The measured n_j -jet rates are then multiplied by $(\mathcal{P}^{-1})_{ij}$ to give the corrected n_i -jet rates. The diagonal terms of these $\mathcal{P}^{-1}$ matrices are dominant for all values of z_γ and y_{cut} ; for example the degree of mixing from 3-jets to 2-jets at detector level is $\leq 10\%$ for $y_{cut} \geq 0.1$ at all values of $z_\gamma \leq 0.95$. The evaluation of $\mathcal{P}^{-1}$ is repeated replacing `ARIADNE` by `HERWIG` and the results agree within Monte Carlo statistics.

Table 2 gives the corrected differential rates in z_γ for each jet topology at $y_{cut} = 0.01$, 0.06, 0.1 and 0.33. The quoted systematic errors are derived from the errors evaluated in the background subtraction and in the photon selection efficiency. In spite of the low purity levels for 2-jet events when $z_\gamma < 0.95$, the uncertainties in the z_γ distributions are dominated everywhere by statistical errors.

Since the non-perturbative part of $D(z_\gamma)$ is naturally associated with the hadronisation process, the measured jet rates are not corrected back to the parton level. In any case, the internal properties of the *accompanying* hadronic jets are not being investigated and it is assumed that these jets characterise the kinematics of the leading partons as described in the QCD calculations. The influence of hadron jet clustering on the measurement of z_γ is taken into account and discussed in the following section.

5 Analysis by Event Topology

5.1 2-jet events

At the primary parton level, 2-jet topologies correspond to either $q\overline{q}\gamma$ where the q and $\overline{q}$ coalesce to form one jet or $q\overline{q}$ where one of the quarks radiates (or fragments into) a photon which remains part of the quark jet. In the absence of radiated gluons, the first case leads to completely isolated photons with $z_\gamma = 1$ whereas the second populates the full z_γ distribution. Thus, it is expected that the quark-to-photon fragmentation function,

$y_{cut} = 0.01$	2-jet events			3-jet events			$\geq$ 4-jet events		
z_γ bin	Rate	$\pm$ Stat.	$\pm$ Syst.	Rate	$\pm$ Stat.	$\pm$ Syst.	Rate	$\pm$ Stat.	$\pm$ Syst.
0.70–0.75	2.01	$\pm$ 0.82	$\pm$ 0.62	2.32	$\pm$ 0.81	$\pm$ 0.39	0.84	$\pm$ 0.51	$\pm$ 0.10
0.75–0.80	0.77	$\pm$ 0.56	$\pm$ 0.43	2.08	$\pm$ 0.67	$\pm$ 0.31	0.36	$\pm$ 0.35	$\pm$ 0.06
0.80–0.85	0.96	$\pm$ 0.56	$\pm$ 0.36	2.15	$\pm$ 0.67	$\pm$ 0.29	0.91	$\pm$ 0.55	$\pm$ 0.08
0.85–0.90	0.85	$\pm$ 0.48	$\pm$ 0.30	3.49	$\pm$ 0.60	$\pm$ 0.23	0.78	$\pm$ 0.31	$\pm$ 0.05
0.90–0.95	0.64	$\pm$ 0.27	$\pm$ 0.18	4.72	$\pm$ 0.51	$\pm$ 0.25	1.73	$\pm$ 0.37	$\pm$ 0.10
0.95–0.99	0.27	$\pm$ 0.20	$\pm$ 0.10	15.57	$\pm$ 1.11	$\pm$ 0.73	3.50	$\pm$ 0.64	$\pm$ 0.19
0.99–1.00	5.84	$\pm$ 1.60	$\pm$ 0.31	97.32	$\pm$ 5.76	$\pm$ 4.66	21.54	$\pm$ 3.07	$\pm$ 1.28

$y_{cut} = 0.06$	2-jet events			3-jet events		
z_γ bin	Rate	$\pm$ Stat.	$\pm$ Syst.	Rate	$\pm$ Stat.	$\pm$ Syst.
0.70–0.75	2.82	$\pm$ 0.83	$\pm$ 0.70	0.62	$\pm$ 0.30	$\pm$ 0.07
0.75–0.80	1.63	$\pm$ 0.64	$\pm$ 0.54	0.01	$\pm$ 0.29	$\pm$ 0.08
0.80–0.85	1.43	$\pm$ 0.54	$\pm$ 0.38	0.08	$\pm$ 0.28	$\pm$ 0.08
0.85–0.90	0.83	$\pm$ 0.42	$\pm$ 0.29	0.70	$\pm$ 0.24	$\pm$ 0.05
0.90–0.95	0.53	$\pm$ 0.24	$\pm$ 0.20	1.16	$\pm$ 0.24	$\pm$ 0.07
0.95–0.99	0.92	$\pm$ 0.25	$\pm$ 0.12	6.10	$\pm$ 0.65	$\pm$ 0.27
0.99–1.00	12.74	$\pm$ 2.32	$\pm$ 0.65	47.87	$\pm$ 4.29	$\pm$ 2.28

$y_{cut} = 0.1$	2-jet events			3-jet events		
z_γ bin	Rate	$\pm$ Stat.	$\pm$ Syst.	Rate	$\pm$ Stat.	$\pm$ Syst.
0.70–0.75	2.95	$\pm$ 0.80	$\pm$ 0.68	0.25	$\pm$ 0.20	$\pm$ 0.03
0.75–0.80	1.68	$\pm$ 0.62	$\pm$ 0.52	0.00	$\pm$ 0.02	$\pm$ 0.04
0.80–0.85	1.25	$\pm$ 0.53	$\pm$ 0.39	0.09	$\pm$ 0.19	$\pm$ 0.04
0.85–0.90	0.81	$\pm$ 0.42	$\pm$ 0.29	0.50	$\pm$ 0.22	$\pm$ 0.04
0.90–0.95	0.49	$\pm$ 0.23	$\pm$ 0.19	0.56	$\pm$ 0.18	$\pm$ 0.04
0.95–0.99	1.10	$\pm$ 0.28	$\pm$ 0.12	3.28	$\pm$ 0.53	$\pm$ 0.16
0.99–1.00	16.06	$\pm$ 2.49	$\pm$ 0.77	24.48	$\pm$ 3.09	$\pm$ 1.19

$y_{cut} = 0.33$	2-jet events		
z_γ bin	Rate	$\pm$ Stat.	$\pm$ Syst.
0.70–0.75	3.09	$\pm$ 0.80	$\pm$ 0.68
0.75–0.80	1.62	$\pm$ 0.61	$\pm$ 0.52
0.80–0.85	1.31	$\pm$ 0.53	$\pm$ 0.40
0.85–0.90	1.04	$\pm$ 0.42	$\pm$ 0.29
0.90–0.95	0.53	$\pm$ 0.23	$\pm$ 0.19
0.95–0.99	1.77	$\pm$ 0.31	$\pm$ 0.14
0.99–1.00	23.68	$\pm$ 2.87	$\pm$ 1.03

Table 2: Normalised Differential Rates ($\times 10^3$) for FSR photons above 5 GeV after background subtraction and acceptance corrections for (top to bottom) $y_{cut} = 0.01$, $y_{cut} = 0.06$, $y_{cut} = 0.1$, $y_{cut} = 0.33$ respectively.

$D(z_\gamma)$, will decrease monotonically towards $z_\gamma = 1$ where the isolated component becomes the principal contribution.

Fig. 3 shows the corrected differential z_γ distributions normalised to the total hadronic event sample for the four values of y_{cut} listed in Table 2. A downward trend is observed up to $z_\gamma = 0.95$, and the isolated photon peak in the final bin $0.99 < z_\gamma < 1.0$ is clearly evident, but then it appears that a fraction of this isolated component populates the $0.95 < z_\gamma < 0.99$ bin. This effect becomes more pronounced with increasing y_{cut}. Both the **ARIADNE** and **HERWIG** parton-shower Monte Carlos ascribe this broadening effect to the association of soft hadrons to the photon jet by the clustering algorithm, whereas no such effect is observed at the parton level. Furthermore, the same Monte Carlo study has been repeated without initial state radiation to confirm that this has no influence on the clustering of soft hadrons to the photon jet. Thus, the conclusion is that at least part of the broadening effect is due to hadronization, and this is the only portion of the z_γ distribution where significant differences between hadron and parton levels appear.

The shapes of the distributions in Fig. 3 are studied by making simple linear fits to the data of the form $a_0 + a_1(1 - z_\gamma)$ restricted to the region $0.7 < z_\gamma < 0.95$. Satisfactory fits are obtained for each y_{cut} which show that a_0 is consistent with zero and a_1 is constant for the upper three values of $y_{cut} \geq 0.06$. Therefore, in the absence of the isolated component, the fragmentation function appears to approach zero at $z_\gamma = 1$ with a slope independent of y_{cut}. Performing a linear fit at $y_{cut} = 0.06$ fixing $a_0 = 0$ yields $a_1 = (7.9 \pm 1.8) \times 10^{-3}$ showing that the significance of the extracted fragmentation function is 4.5 standard deviations.

At the Z, the measured fragmentation function is the average of the $D(z_\gamma)$ functions for the combination of the 2 u-type and 3 d-type quark flavours weighted by their respective electro-weak couplings and electric charges. Thus, $D(z_\gamma)$ is obtained from the normalised differential 2-jet cross section:

$$\frac{1}{\sigma_{had}} \frac{d\sigma(\text{2-jet})}{dz_\gamma} = D(z_\gamma) G_{LEP}$$

where G_{LEP} is twice the ratio of the FSR correction to the total hadronic cross section at the Z, given by:

$$G_{LEP} = 2 \left(\frac{\alpha}{2\pi} \right) \frac{(2e_u^2 \Gamma_u + 3e_d^2 \Gamma_d)}{\Gamma_{had}}$$

The factor 2 accounts for the two quarks produced in the Z decay. From currently measured values for these parameters [17] $G_{LEP} = 2.51 \times 10^{-4}$. This normalisation does not take into account any other source of flavour dependence in the fragmentation function.

5.1.1 Comparison of $D(z_\gamma)$ with a Leading-Log calculation

The differential 2-jet distributions are compared with a theoretically parametrised fragmentation function [9] which has been widely used to determine the level of quark bremsstrahlung in prompt photon data at the hadron colliders [18]. In these experiments, a residual high z_γ quark fragmentation contribution appears in the prompt photon

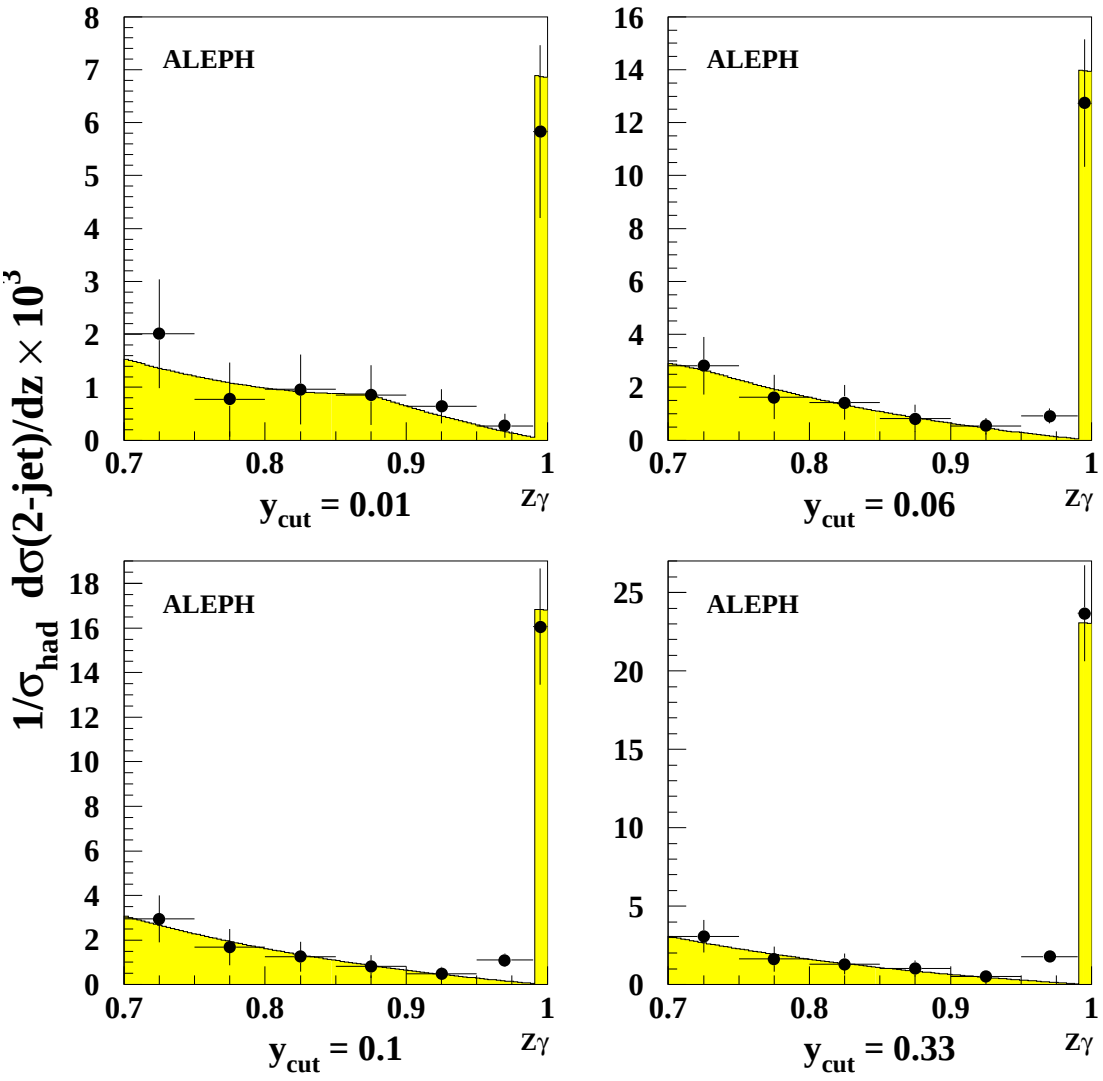

Figure 3: Comparison of the 2-jet rates measured for 4 values of y_{cut} to an universal fragmentation function calculated using $B(z_\gamma\,,\mu_0) = -1 - \log(s/2\mu_0^2)$ with $\mu_0 = 0.14$ GeV (see text).

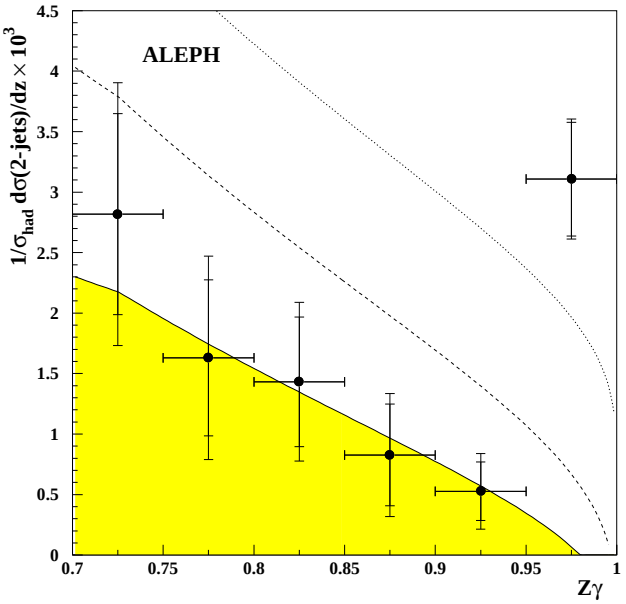

Figure 4: Comparison of the measured $D(z_\gamma)$ function extracted from the 2-jet rates at $y_{cut} = 0.06$ to the Duke-Owens fragmentation function for $Q = p_T$ (dashed), and $Q = M_Z$ (dotted) with $\Lambda = 0.2$ GeV. The continuous curve shows the result of a fit of the Duke-Owens function with $Q = p_T$ giving $\Lambda = 1.30^{+0.70}_{-0.45}$ GeV with $\chi^2/4 = 0.48$.

signal because some hadronic energy is necessarily allowed to accompany the isolated photon, usually defined by a geometrical cone. This theoretical parametrisation consists of a dominant leading-logarithm term, D^{LL}, which is proportional to $\log(Q^2/\Lambda^2)$ with a coefficient parametrised in z_γ. Here, Q represents a scale which is characteristic of the transverse momentum of the photon with respect to the parent quark. In this analysis, the FSR photons are not identified on an event-by event basis. Therefore, the scale has been chosen to be the *maximum* transverse momentum, p_T, which is given by:

$$p_T = \sqrt{\frac{z_\gamma\,(1-z_\gamma)^2}{(1+z_\gamma)}\ s}$$

when $y_{cut} \geq 0.06$. In this case, Q ranges from 17 GeV at $z_\gamma = 0.7$ to zero at $z_\gamma = 1$. The lower cut-off scale, Λ, is chosen to be the characteristic hadronization scale which is set initially to be 0.2 GeV [19]. Fig. 4 shows the comparison between the theoretical prediction multiplied by G_{LEP} (dashed curve) and the data at $y_{cut} = 0.06$. In this case, the data points above $z_\gamma = 0.95$ are combined into one bin to take account of the observed broadening of the isolated component. This point is not to be included in the comparison. The prediction follows the shape of the measured distribution but the rate is too large. An acceptable fit to the data in the range $0.7 < z_\gamma < 0.95$ can be obtained allowing Λ to vary. This is shown in Fig. 4 from which a value of $1.30^{+0.70}_{-0.45}$ GeV is found.

Choosing $Q = M_Z$ gives a poorer fit to the data for any value of Λ indicating that the photon transverse momentum which varies with z_γ appears to give a better choice of

scale. However, fits to a more complete next-to-leading log calculation which includes $\log(1-z_\gamma)$ terms are required before this observation can be confirmed.

5.1.2 Parametrisation of the Non-Perturbative Component of $D(z_\gamma)$

Following the leading order formalism of ref [10] developed in a $\overline{MS}$ renormalisation scheme the inclusive quark-to-photon fragmentation function $D(z_\gamma)$ can be written in the following way at a CM energy of $\sqrt{s}$:

$$D(z_\gamma) = D_{np}(z_\gamma, \mu_F) + \frac{1+(1-z_\gamma)^2}{z_\gamma} \log\left(\frac{s}{\mu_F^2}\right) + \widehat{D}_{inv}(z_\gamma) \qquad (1)$$

where the non-perturbative component, D_{np}, is separated from the perturbative part of the fragmentation function at an arbitrary factorisation scale μ_F. Thus, $D(z_\gamma)$ is the sum of a non-perturbative term D_{np}, a scale-dependent perturbative contribution and a scale invariant part $\widehat{D}_{inv}(z_\gamma)$. The latter can be written as

$$\widehat{D}_{inv}(z_\gamma) = \frac{1+(1-z_\gamma)^2}{z_\gamma} \log\left(\frac{z_\gamma(1-z_\gamma)^2}{1+z_\gamma}\right) + f(z_\gamma, y_{cut}) + \frac{1}{2} R_\Delta(y_{cut})\delta(1-z_\gamma),$$

where $f(z_\gamma, y_{cut})$ is a known regular function with $f(z_\gamma = 1) = 1$ and R_Δ the perturbative component for isolated photon production without accompanying partonic energy. For $z_\gamma > 0.7$, f becomes independent of y_{cut} when $y_{cut} \geq 0.07$ because then the photon always combines with its radiating quark to form a jet. Therefore, apart from the R_Δ contribution, $D(z_\gamma)$ is expected to be independent of y_{cut} in this region as is observed.

In the leading order formalism of [10] the function $D_{np}(z_\gamma, \mu_F)$ can be parametrized as

$$D_{np}(z_\gamma, \mu_F, \mu_0) = A(z_\gamma, \mu_F/\mu_0) + B(z_\gamma, \mu_0)$$

with

$$A = \frac{1+(1-z_\gamma)^2}{z_\gamma} \log\left(\frac{\mu_F^2}{\mu_0^2(1-z_\gamma)^2}\right).$$

The A-term is an exact solution of the leading order evolution equation for D_{np}, which having the same coefficient in the logarithms as found in the perturbative part cancels the μ_F-dependence and the negative divergence at $z_\gamma = 1$. The second term, $B(z_\gamma, \mu_0)$, is required in order to specify the starting value of D_{np} at $\mu_F = \mu_0$ interpreted as a lower cut-off mass scale below which the perturbative approach breaks down. Although only leading order, this parametrisation has the attractive property of producing an expression for $D(z_\gamma)$ which does not depend on the factorisation scale.

Inserting this parametrisation into equation (1) yields (for large z_γ)

$$D(z_\gamma) = \frac{1+(1-z_\gamma)^2}{z_\gamma} \log\left(\frac{z_\gamma}{1+z_\gamma}\frac{s}{\mu_0^2}\right) + B(z_\gamma, \mu_0) + f(z_\gamma) + \frac{1}{2} R_\Delta \delta(1-z_\gamma) \qquad (2)$$

where the free parameters to be determined are the cut-off scale μ_0 and the function $B(z_\gamma, \mu_0)$. The two highest z_γ bins are combined into one bin with $z_\gamma > 0.95$ to take into

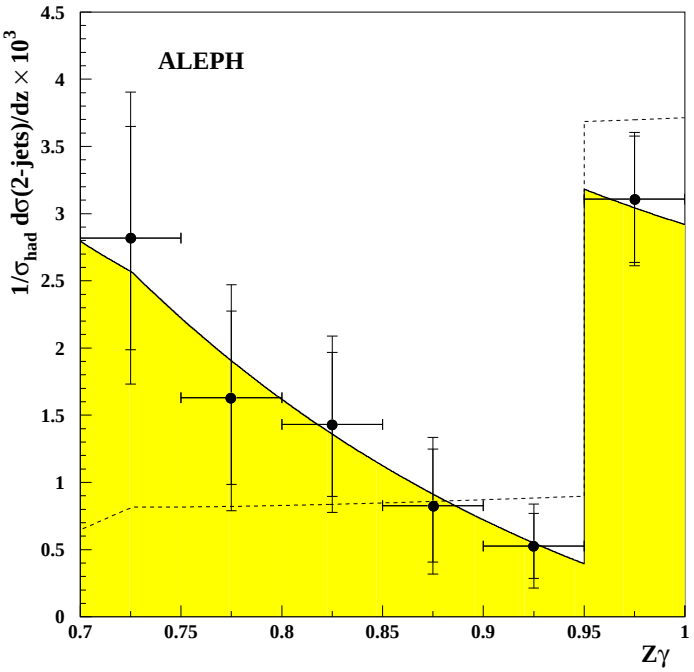

Figure 5: Fits to the quark-to-photon fragmentation function for y_{cut}=0.06: the solid and dashed curves show the results for the parametrisations $B(z_\gamma\,,\mu_0) = C$ and $B(z_\gamma\,,\mu_0) = 0$ respectively. The R_Δ contribution is smeared uniformily from $z_\gamma = 0.95$ to 1.0.

account the observed broadening of the isolated component. It is then assumed that the isolated component in the data is concentrated entirely in this bin. Since the magnitude and z_γ dependence of $B(z_\gamma\,,\mu_0)$ are unknown, various parametrisations have been tried in fitting $D(z_\gamma)$ to the six data points in the range $0.7 < z_\gamma < 1.0$. The parametrisations tried for $B(z_\gamma\,,\mu_0)$ include zero, a constant C, $C_1 + C_2(1-z_\gamma)$, and $C + (1-z_\gamma)^\beta$. They show that $B(z_\gamma\,,\mu_0) = 0$ does not give a sensible fit, whereas the data cannot differentiate between the acceptable quality of the fits obtained from the other three parametrisations. This behaviour is illustrated in Fig. 5 where for simplicity $B(z_\gamma\,,\mu_0) = C$ is chosen as providing an adequate representation of the data. The shape of $D(z_\gamma)$ is well described with the evolution equation alone, but the normalisation to the data requires a constant negative off-set. The corresponding double parameter fit having a $\chi^2/4 = 0.24$ gives $\mu_0 = 0.22^{+1.3}_{-0.19}$ GeV and $C = -12.1 \pm 4.3$ where statistical and systematic errors are combined in quadrature.

The values of C and μ_0 thus found are strongly correlated. This is related to the observation made earlier that the fragmentation function approaches zero at $z_\gamma = 1$ when the isolated component, R_Δ, is disregarded. In fact, imposing the condition $D(z_\gamma = 1) = R_\Delta/2$ yields the following relation between C and μ_0

$$C = -1 - \log\left(\frac{s}{2\mu_0^2}\right). \tag{3}$$

The fit results are found to be in very good agreement with this simple relation. A more precise value of μ_0 can be obtained by performing a single parameter fit to the data using the parametrisation of $B(z_\gamma\,,\mu_0) = C$ where the latter is constrained by the above relation. The best value is found to be:

$$\mu_0 = 0.14^{+0.21+0.22}_{-0.08-0.04}\ \text{GeV} \quad \text{with} \quad \chi^2/5 = 0.37.$$

The single parameter fit was repeated for y_{cut} values of 0.008, 0.02, 0.1 and 0.33 and consistent results are found showing that over this range, the non-perturbative term, D_{np}, is universal as expected, and any y_{cut} dependence in the perturbative parts, including the isolated component, are adequately described by the leading order calculations. The results of these fits are shown in Fig. 3.

5.1.3 Isolated photon region: $0.95 < z_\gamma < 1$

The *integrated* rates above $z_\gamma = 0.95$ are now compared with $D(z_\gamma)$ described by equation (2) where the single parameter fitted value of $\mu_0 = 0.14$ GeV and the corresponding value for C are substituted. Fig. 6 shows the result of this comparison as a function of y_{cut}. The agreement is adequate over the full range of y_{cut}. It should be noted that the predictions of this leading order formalism for the 2-jet rate contain perturbative components which are derived from a pure QED calculation. In previous two-step analyses [1], a large α_S dependent next-to-leading order QCD correction was needed to describe the 2-jet rate for isolated photons.

Fig. 6 also shows that `JETSET` falls substantially below the data at all values of y_{cut} in contrast to `ARIADNE` and `HERWIG` (not shown) where the agreement is satisfactory at high y_{cut}.

5.2 3- and $\geq$4-jet event rates

As shown in Fig. 1, the z_γ distributions for 3- and $\geq$4-jet events are quite different from the 2-jet topologies, being dominated by the isolated photon peak near $z_\gamma = 1$. For the 3-jet topology, this is not unexpected since for $z_\gamma < 1$ the quark fragmentation function now appears at next-to-leading order, while the gluon fragmentation function, which appears at lowest order from the $Z \to q\bar{q}g$ process, is expected to be small when $z_\gamma > 0.7$. These fragmentation processes are suppressed by a further order of α_S in the 4-jet case and hence are not calculated in the following QCD predictions.

The acceptance corrected z_γ distributions are compared at each value of y_{cut} with the same $\mathcal{O}(\alpha\alpha_S)$ calculation [10] which now includes the non-perturbative part of $D(z_\gamma)$ measured from the 2-jet rate. This treatment is implemented in an updated version of the matrix element Monte Carlo program `EEPRAD` [2] which allows the experimental photon energy cut at 5 GeV to be applied. The only free parameter is α_S. Fig. 7 shows the comparison between the corrected 3-jet data and `EEPRAD` at $y_{cut} = 0.01$, with $\alpha_S = 0.17$ and any gluon fragmentation contribution ignored. As seen earlier in the 2-jet case, the isolated photon component in the data extends down to $z_\gamma \sim 0.95$. However, in this case `EEPRAD` predicts a perturbative contribution to the broadening of the isolated component

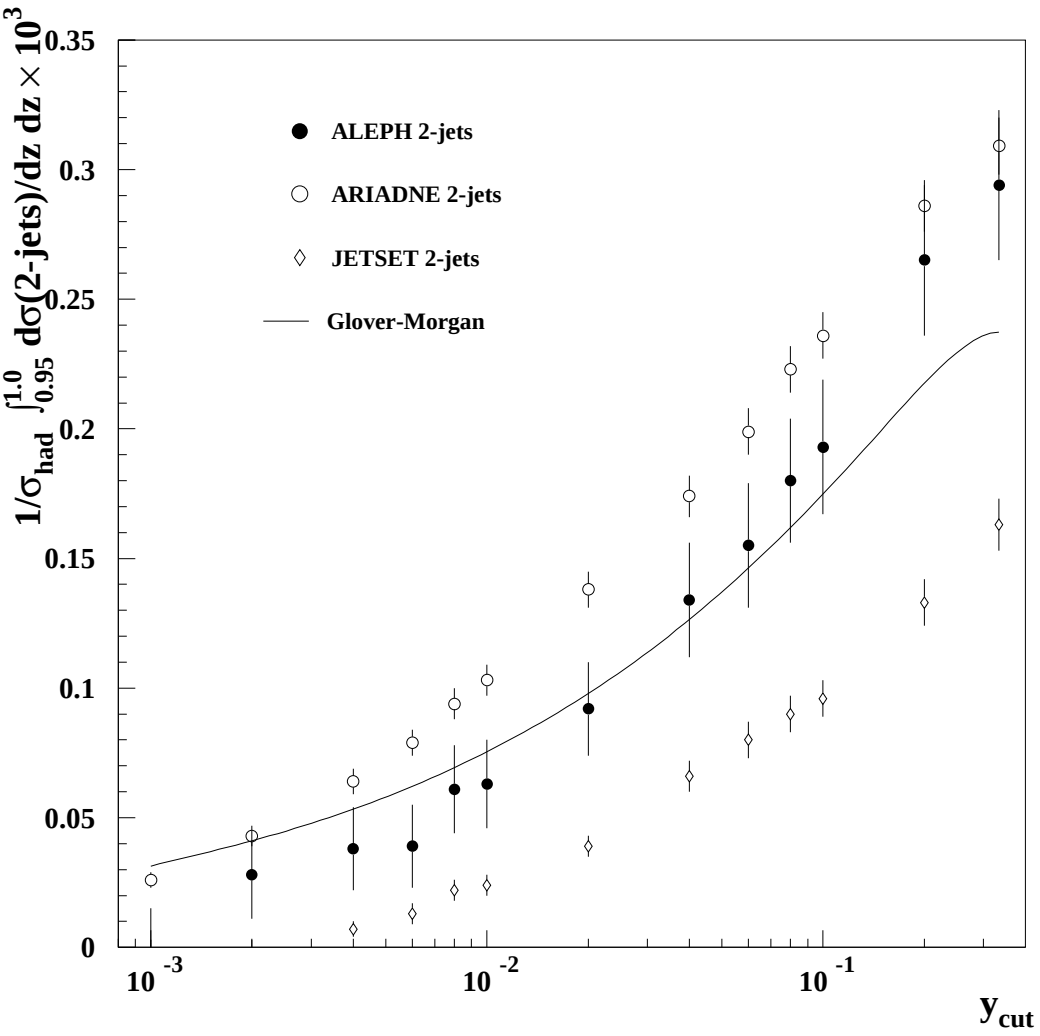

Figure 6: Integrated 2-jet rate above $z_\gamma = 0.95$ as function of y_{cut}, compared with the full QCD calculation including the fitted non-perturbative component of the $D(z_\gamma)$ function.

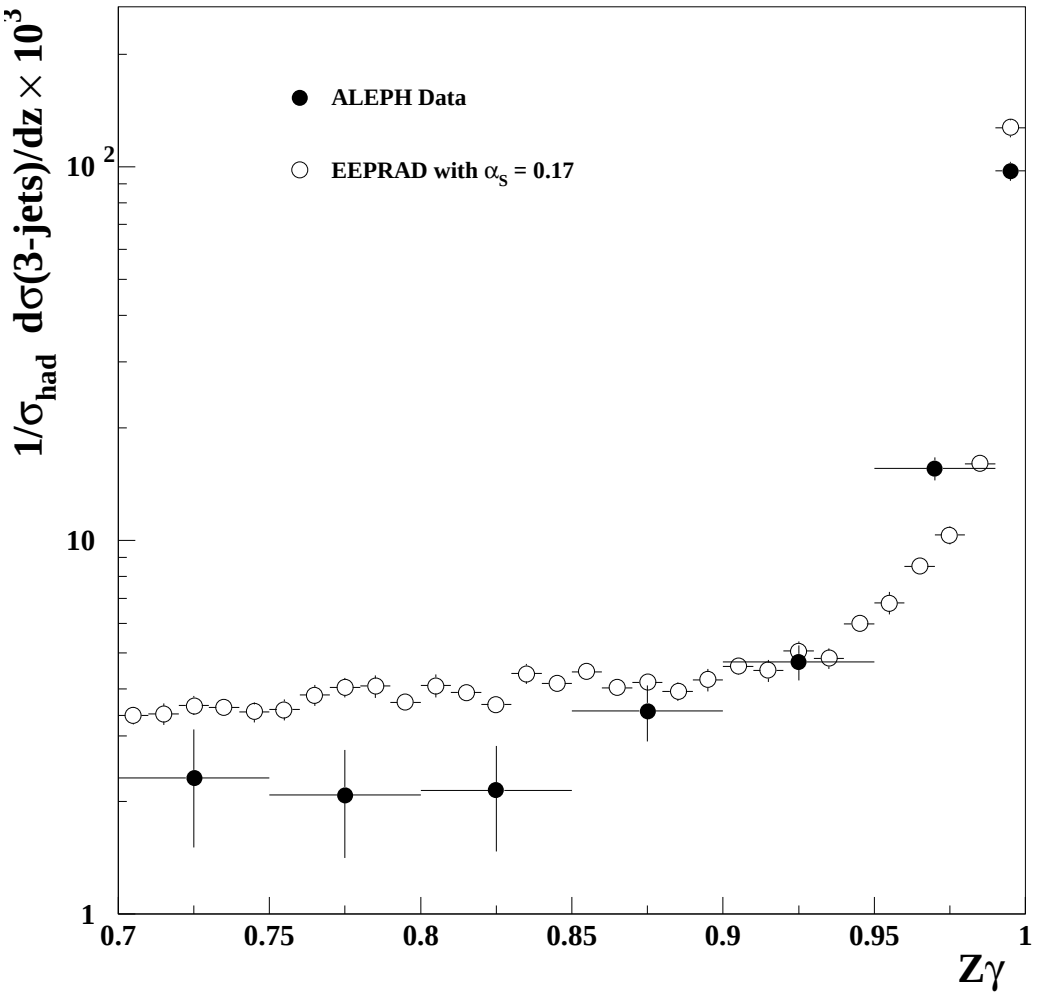

Figure 7: The 3-jet differential rates for $y_{cut} = 0.01$ compared with the $\mathcal{O}(\alpha\alpha_S)$ calculation which includes the non-perturbative part of the $D(z_\gamma)$ fragmentation function measured from the 2-jet rate.

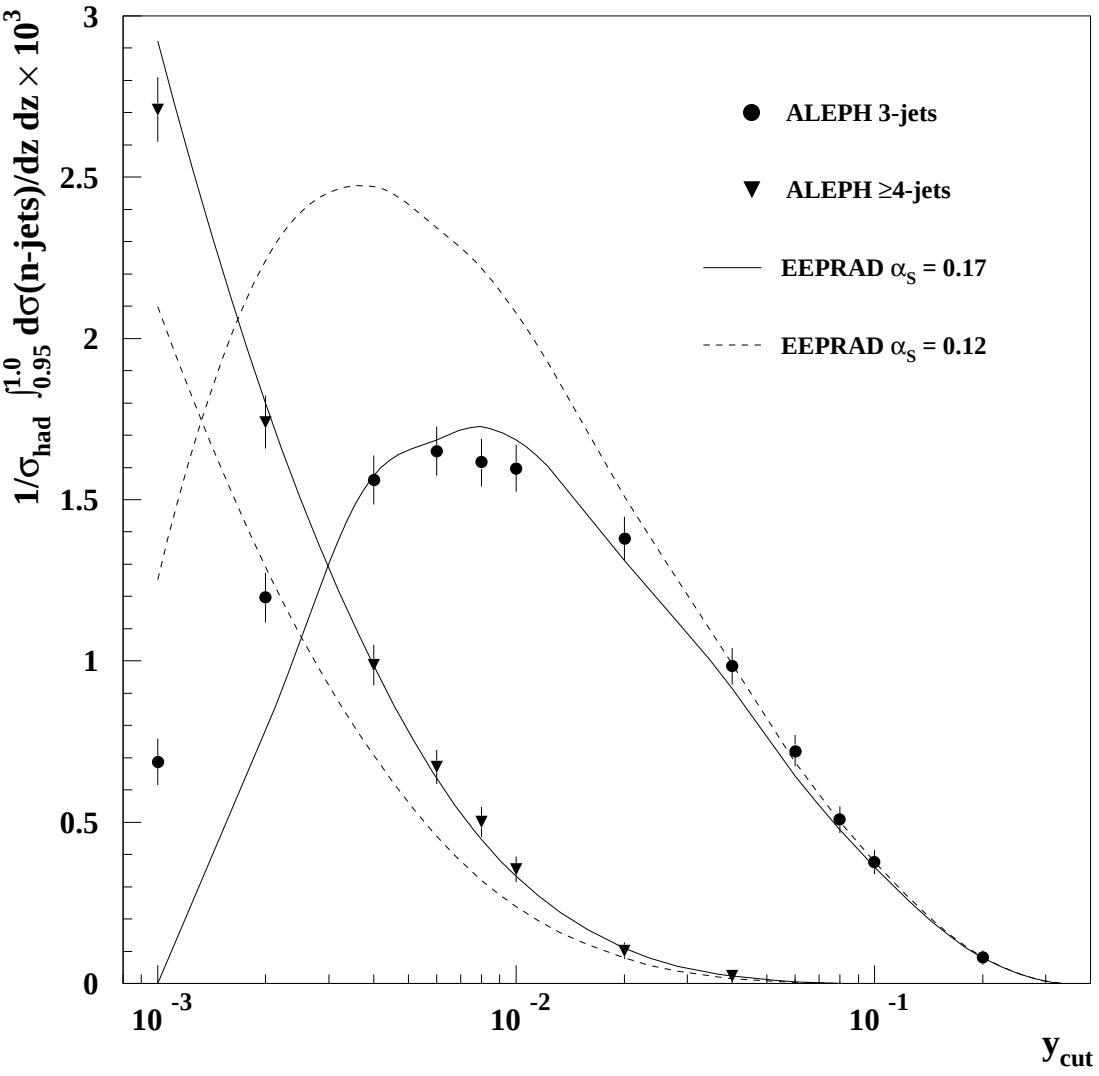

Figure 8: The 3-jet and $\geq$ 4-jet integrated rates with $z_\gamma \geq 0.95$ as a function of y_{cut} , compared with EEPRAD predictions.

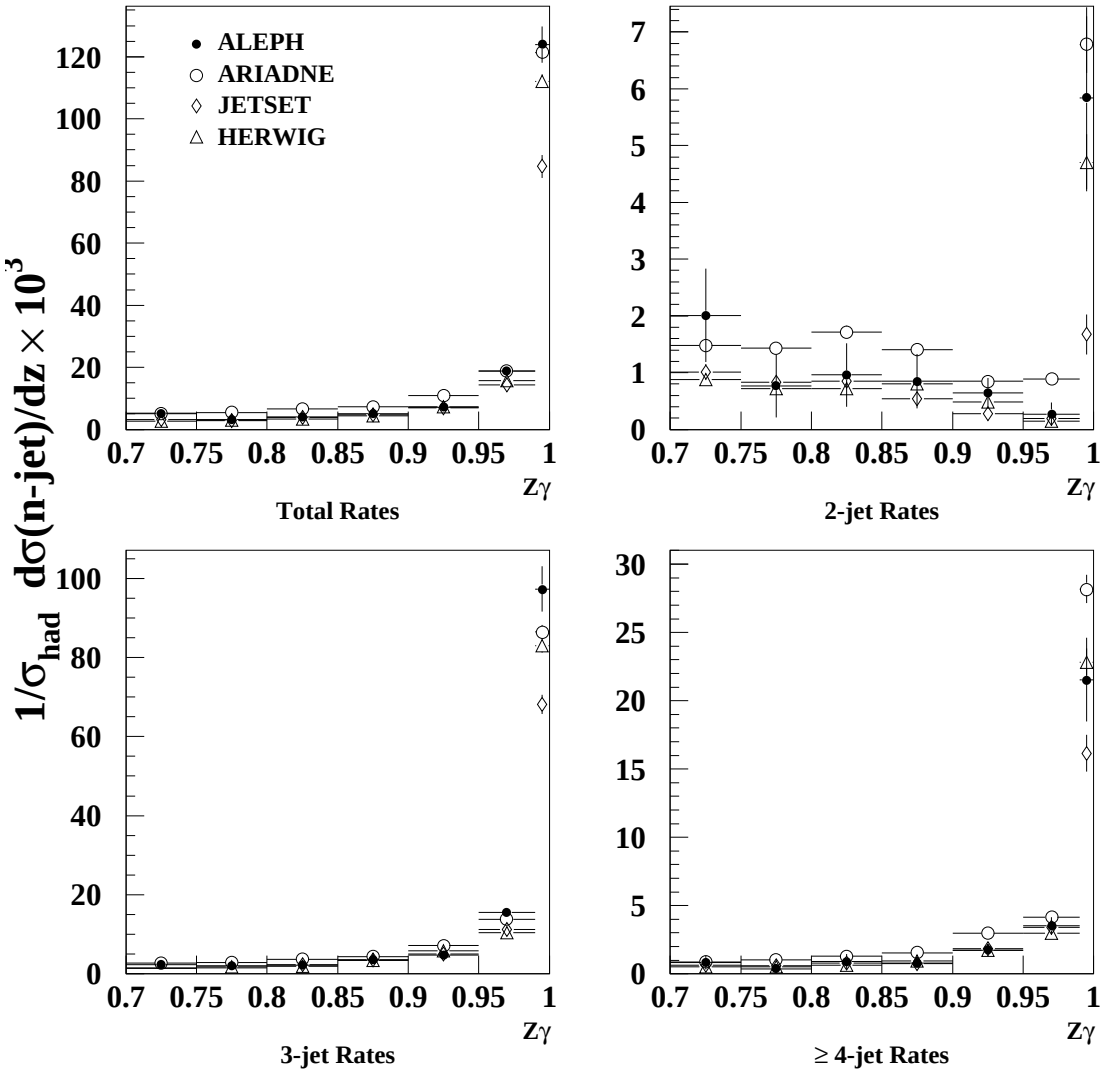

Figure 9: Differential n-jet rates as a function of z_γ for $y_{cut} = 0.01$, compared with the predictions of ARIADNE, JETSET and HERWIG.

although it appears that the dominant effect is still non-perturbative hadronization as before. Thus, to compare with the predictions of **EEPRAD**, the rates are integrated above $z_\gamma = 0.95$ with the non-perturbative parts of the fragmentation function included. Fig. 8 shows the results of this comparison. Effectively, the value of $\alpha_S = 0.17$ compensates for the missing higher orders and other scheme dependent factors neglected in **EEPRAD**. Both the predicted 3-jet and 4-jet rates follow the data closely down to very low values of $y_{cut} \sim 0.003$.

It should be noted, however, that this choice of α_S leads to a good description of the data only above $z_\gamma = 0.95$ where the isolated component dominates. In the lower z_γ fragmentation region, Fig. 7 shows that this leading order description is inadequate.

5.3 Comparison with Monte Carlo Event Generators

Further comparisons between the differential n-jet rates as a function of z_γ and the predictions of **ARIADNE**, **JETSET** and **HERWIG** are shown in Fig. 9 for $y_{cut} = 0.01$. They demonstrate that even though **ARIADNE** agrees best with the data when $z_\gamma > 0.99$, its predictions are too high elsewhere for all jet topologies. Conversely, **JETSET** follows the measured differential rates well for $z_\gamma < 0.99$ but consistently lies below the data in predicting the isolated component at $z_\gamma = 1$. However, it is interesting to note that the level of this discrepancy diminishes with the accompanying jet multiplicity. **HERWIG** gives the best overall agreement.

6 Conclusions

The high z_γ part of the quark-to-photon fragmentation function, $D(z_\gamma)$, has been measured from hadronic 2-jet events at the Z by a democratic analysis where the photon was treated equally with the other particles in the jet reconstruction. It was then shown that the measured $D(z_\gamma)$ function can be described by a factorisation scale independent QCD leading order prescription with non-perturbative contributions in which the only free parameter is a cut-off mass scale μ_0. After fitting this prescription to the data to determine μ_0, a satisfactory description of all aspects of the measured 2-jet rates can be found. Next-to-leading $\mathcal{O}(\alpha_S)$ corrections are not required, in contrast to earlier analyses which used a two-step approach to classify the photon jet.

In addition, a good description of the other dominant n-jet rates can be obtained using the same formalism to $\mathcal{O}(\alpha\alpha_S)$ provided the non-perturbative fragmentation components evaluated from the 2-jet rates are included, and due account is taken of hadronization effects near $z_\gamma = 1$.

Acknowledgements

We are very grateful to Nigel Glover and Andrew Morgan for many useful discussions, and to Jeff Owens for a valuable contribution. We wish to thank our colleagues from the accelerator divisions for the successful operation of LEP. We are indebted to the engineers

and technicians in all our institutes for the good performance of ALEPH. Those of us from non-member states thank CERN for its hospitality.

Note added

Upon completion of this paper, it was realized [20] by the authors of ref [10] that a single power of $(1-z_\gamma)$ in the logarithm appearing in the function $A(z_\gamma, \mu_F/\mu_0)$ is better motivated than the $(1-z_\gamma)^2$ used here and in ref [10]. However, this is of no physical consequence since the fitting region in z_γ does not constrain the large logarithms in any way and can be considered as equivalent to a redefinition of the a priori unknown function $B(z_\gamma, \mu_0)$.

References

[1] P.D. Acton et al., OPAL Collaboration, *Z. Phys.* **C58** (1993) 405,
D. Buskulic et al., ALEPH Collaboration, *Z. Phys.* **C57** (1993) 17,
P. Abreu et al., DELPHI Collaboration, *Z. Phys.* **C53** (1992) 555,
O. Adriani et al., L3 Collaboration, *Phys. Lett.* **B292** (1992) 472.

[2] E.W.N. Glover and W.J. Stirling, *Phys. Lett.* **B295** (1992) 128.

[3] G. Kramer and H. Spiesberger, *"Matrix element calculation of quark bremsstrahlung in $\mathcal{O}(\alpha\alpha_S)$"*, DESY 92-022 (1992), contribution to the Workshop on Photon Radiation from Quarks, Annecy, France, 1991.

[4] T. Sjostrand and M. Bengtson, *Comput. Phys. Comm.* **43** (1987) 367.

[5] G. Marchesini et al., *Comput. Phys. Comm.* **67** (1992) 465.

[6] L. Lonnblad, *Comput. Phys. Comm.* **71** (1992) 15.

[7] P. Mättig, H. Spiesberger and W. Zeuner, *Z. Phys.* **C60** (1993) 613.

[8] Y. Dokshitzer, Contribution to the Workshop on Jets at LEP and HERA, *J. Phys.* **G17** (1991) 1441.

[9] D.W. Duke and J.F. Owens, *Phys. Rev.* **D26** (1982) 1600.

[10] E.W.N. Glover and A.G. Morgan, *Z. Phys* **C62** (1994) 311.

[11] D. Decamp et al., ALEPH Collaboration, *Nucl. Instrum. Methods* **A294** (1990) 121.

[12] D. Decamp et al., ALEPH Collaboration, *Z. Phys.* **C53** (1992) 1.

[13] D. Buskulic et al., ALEPH Collaboration, *Nucl. Instrum. Methods* **A360** (1995) 481.

[14] D. Buskulic et al., ALEPH Collaboration, *Z. Phys.* **C55** (1992) 209.

[15] D. Buskulic et al., ALEPH Collaboration, *Z. Phys.* **C66** (1995) 355.

[16] S. Jadach, B. Ward and Z. Was, *Comput. Phys. Comm.* **66** (1991) 276.

[17] The LEP Collaborations and the LEP Electroweak Working Group, CERN-PPE/93-157.

[18] F. Abe et al., CDF Collaboration, *Phys. Rev.* **D48** (1993) 2998.

[19] H. Baer, J. Ohnemus and J.F. Owens, *Phys. Rev.* **D42** (1990) 61.

[20] N. Glover, private communication.